Eur. Phys. J. B **67**, 483–494 (2009)
DOI: 10.1140/epjb/e2009-00047-1

THE EUROPEAN PHYSICAL JOURNAL B

Regular Article

Electronic structure of CeRhX (X = Sn, In)

M. Gamża[1,a], A. Ślebarski[1,b], and H. Rosner[2,c]

[1] Institute of Physics, University of Silesia, 40-007 Katowice, Poland
[2] Max-Planck Institute for Chemical Physics of Solids, 01187 Dresden, Germany

Received 30 July 2008 / Received in final form 12 November 2008
Published online 14 February 2009 –

Abstract. Electronic structure of the compounds CeRhIn and CeRhSn have been studied by the X-ray photoemission spectroscopy (XPS) and ab initio band structure calculations. CeRhSn shows the non-Fermi liquid characteristics at low temperatures, while CeRhIn exhibits a Fermi-liquid ground state. At ambient temperature the XPS data reveal an intermediate valence state of Ce ions in both systems. The Ce core-level XPS spectra are very similar and indicate the strong coupling of the Ce $4f$ and the conduction band states ($\Delta \approx 100$ meV). The valence band spectra we interpret with the help of ab initio calculations as well as using the results for the reference compounds LaRhIn and LaRhSn. The comparative analysis of the theoretical band structures and charge density plots reveal the changes in chemical bonding and the hybridization between the Ce $4f$ and the other valence states introduced by the replacement of In by Sn atoms. The more covalent character of the chemical bonding in the stannides is in line with the smaller thermal expansion. Finally, for CeRhIn we found a typical temperature dependence of the crystal lattice, while CeRhSn shows distinct anomaly at about 120 K, presumably related to the change in planar Ce–Rh bonds.

PACS. 79.60.-i Photoemission and photoelectron spectra – 71.20.LP Intermetallic compounds – 71.27.+a Strongly correlated electron systems; heavy fermions

1 Introduction

Over the past two decades, much attention has been devoted to the ternary compounds CeMX (M = transition metal and X = p-element) crystallizing within the hexagonal ZrNiAl-type structure. The physical picture of the ground state properties and excitation spectra within this family of compounds is far from being fully understood and is still under intense debate [1–21].

The ground state properties of these systems are governed mainly by the strong antiferromagnetic exchange coupling J_{s-f} of the Ce $4f$ moments with conduction band states. This coupling gives rise to two competing mechanisms: the on-site Kondo screening of the localized Ce $4f$ moments by the band states and the long-range Ruderman-Kittel-Kasuya-Yosida (RKKY) interactions between the local $4f$ moments mediated by the conduction electrons. Besides, the ZrNiAl-type structure induces topological frustration of magnetic interactions due to the triangular coordination of the Ce ions forming the quasi-Kagome lattice within the ab-planes. The frustration, together with the strong exchange coupling J_{s-f}, results in a rich variety of unusual ground states within this family of isostructural compounds.

CeNiAl [2,3], CeRhIn [4–6] and CeIrSn [7] are non-magnetic valence-fluctuation systems with very high Kondo temperatures of 1000 K for CeNiAl and at least 300 K for CeRhIn. For CePtIn the dominance of the Kondo effect over the RKKY interactions leads to a non-magnetic heavy-fermion ground state with $T_K \sim 11$ K [8,9]. In contrast, for CePdIn [8,10], CePdAl [11,12], CePtPb [13] and CeCuAl [3,14] the interplay of the Kondo screening and the long-range magnetic interactions with $T_N \sim T_K$ results in an antiferromagnetic ordering accompanied by an enhanced electron mass. However, the detailed neutron scattering studies revealed, that the magnetic structure of CePdAl is partially ordered and one third of Ce atoms remain paramagnetic below $T_N = 2.7$ K, which can be attributed to frustration effects [11]. Recent results suggest that at low temperatures the Ce atoms with disordered magnetic moments are in a heavy fermion state [12]. In turn, CeAuIn orders magnetically below 6 K and forms a simple antiferromagnetic structure with a propagation vector $k = (0\ 0\ 1/2)$, in which the Ce magnetic moments of 1.2(1) μ_B lie in ab-planes [15].

Among the discussed group of Ce-based intermetallics, CeRhSn has attracted special interest due to its non-Fermi

[a] e-mail: monikag3@o2.pl
[b] e-mail: andrzej.slebarski@us.edu.pl
[c] e-mail: rosner@cpfs.mpg.de

Table 1. Comparison of the crystallographic data for the compounds RERhX (RE = La, Ce; X = In, Sn).

Atoms		x	y	z	
RE	$3g$	x_{RE}	0	0.5	
Rh1	$1b$	0	0	0.5	
Rh2	$2c$	1/3	2/3	0	
X	$3f$	x_X	0	0	
Compound	Data from	a (Å)	c (Å)	x_{RE}	x_X
LaRhIn	our data	7.6155(5)	4.1305(4)	–	–
	[24]	7.618	4.123	0.585	0.245
	[5]	7.610	4.129	–	–
CeRhIn	our data	7.5512(6)	4.0472(7)	–	–
	[5]	7.547	4.05	–	–
	[25]	7.552	4.055	–	–
	[26]	7.555	4.055	–	–
LaRhSn	[42]	7.4874(5)	4.2216(3)	0.58377(9)	0.24490(9)
	[27]	7.478	4.223	–	–
CeRhSn	our data	7.4483(8)	4.0806(9)	–	–
	[17]	7.443(2)	4.089(2)	0.58567(8)	0.24999(9)
	[42]	7.458(1)	4.0862(9)	0.58556(11)	0.24988(10)
	[16]	7.4491(2)	4.0814(1)	0.5868(5)	0.2490(3)
	[16]*	7.4248(1)	4.0645(1)	0.5853(5)	0.2506(3)
	[28]	7.448(2)	4.0800(9)	–	–

* Data at a temperature $T = 1.5$ K.

liquid (NFL) behaviour at low temperatures indicated by electrical resistivity, specific heat and magnetic susceptibility measurements [16,17]. The Griffiths-McCoy model has been successfully applied for this compound and provides the description of its NFL properties [18]. According to this theory, the competition between the Kondo effect and the RKKY interactions in the presence of atomic disorder leads to small magnetically ordered clusters in a paramagnetic phase (Griffiths phases [22]), where dynamics can dominate the low temeprature thermodynamic properties due to tunneling between different configurations [23]. Hence, CeRhSn is supposed to be located on the border between a nonmagnetic and a magnetically ordered ground state, presumably in the vicinity of the AFM instability, as indicated by the NMR results [19]. Simultaneously, the anomalous volume deviation from the usual lanthanide contraction, the overall magnetic susceptibility and resistivity data as well as photoemission spectra [16,20,21] strongly suggest valence fluctuations in this compound. Thus, CeRhSn could be a rare example of a system, where NFL behaviour coexists with a valence fluctuation state of Ce. In contrast, for the compound CeRhIn various experimental methods unanimously revealed a non-magnetic Fermi-liquid ground state with a high Kondo temperature of the order of 300 K and an intermediate-valence behaviour of Ce [4–6].

To get deeper insight into the interactions responsible for the change in ground state properties between CeRhIn and CeRhSn, we performed a detailed study of their electronic structure based on the X-ray photoemission spectroscopy (XPS) experiments at ambient temperature and ab initio band structure calculations. The main purpose of our systematic investigation is to clarify the changes in the character of the Ce $4f$ states and chemical bonding introduced by the replacement of In by Sn atoms. For a proper comparison we measured the XPS spectra for the compounds CeRhIn and CeRhSn under the same conditions, including LaRhIn as a nonmagnetic reference system. We analyse also the temperature dependence of lattice parameters for both CeRhIn and CeRhSn [16] in order to get information about the changes in the bonding situation depending on the temperature for these compounds.

2 Methods

2.1 Experimental

Polycrystalline samples of CeRhSn, CeRhIn and LaRhIn were prepared by arc melting stoichiometric amounts of the elemental metals (Ce 99.99 wt.%, La 99.99 wt.%, Rh 99,9 wt.%, Sn 99,995 wt.%, In 99,995 wt.%) on a water cooled cooper hearth in an ultra-high purity Ar atmosphere with an Al getter (heated above the melting point). Each sample was remelted several times to promote homogeneity and annealed at 800 °C for 7 days in an evacuated quartz tube.

The quality of the samples was examined by the powder X-ray diffraction (XRD) analysis. The measurements were performed on a Siemens D-5000 diffractometer using Cu K_α radiation. The XRD patterns revealed that all investigated compounds crystallize in a hexagonal structure (space group: $P\bar{6}2m$), which is consistent with previous reports [5,16,17,24–28]. The ambient temperature lattice parameters acquired from the diffraction patterns using the POWDER-CELL program [29] are in agreement with those previously reported (Tab. 1). The samples were found to be in good quality. Few additional very weak Bragg peaks were detected, similar in each XRD spectrum.

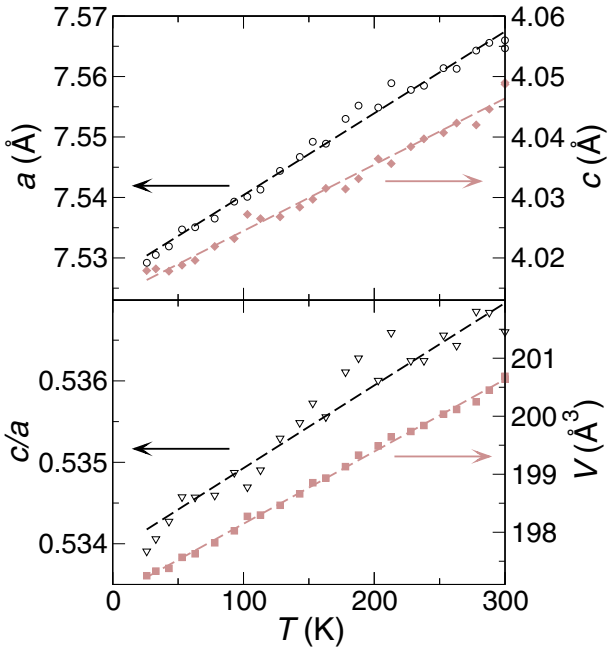

Fig. 1. (Color online) The temperature dependence of the lattice parameters, their ratio c/a and the unit cell volume for the compound CeRhIn. The dashed lines represent the linear fits of the experimental data, with the exception of the c over a ratio where the straight line was obtained as ratio of the linear fits of the $a(T)$ and $c(T)$ data.

We assign them to a small amount of an unidentified minority phase ($\lesssim$2%). Its presence is irrelevant for the RE core-level and valence band XPS measurements, since such experiments are not sensitive to even several percent of impurity phase.

For CeRhIn we performed additional XRD experiments in order to determine the temperature dependences of the lattice parameters. The following Bragg reflections: 002, 311, 400, 212, 302, 410, 321 and 222 were recorded at different temperatures. The positions of the peaks were established by a least-squares curve fitting code using a Lorentzian profile. Lattice parameters were refined using the Checkcell program [30]. The results are plotted in Figure 1.

The XPS spectra were obtained with monochromatized Al K_α radiation at ambient temperature using a PHI 5700 ESCA spectrometer. The total energy resolution was about 0.4 eV. Polycrystalline samples were broken under a high vacuum of 6×10^{-10} Torr immediately before measuring the spectra. Binding energies were referenced to the Fermi level ($\epsilon_F = 0$). Calibration of the spectra was performed according to reference [31].

2.2 Computational

Electronic band structure calculations were carried out using the full potential linearized augmented plane-wave (FP-LAPW) method [32] by the WIEN2k computer code [33]. In this method the unit cell is divided into non-overlapping muffin-tin spheres centered at the atomic sites and an interstitial region. The muffin-tin radii were chosen to be of 2.5 a.u. for Ce and La, 2.4 a.u. for Rh and 2.5 a.u. for In and Sn. Inside the atomic spheres, partial waves were expanded up to $l_{max} = 10$, while the number of plane waves in the interstitial region was limited by the cutoff at $K_{max} = 9.0/R_{MT}$, where R_{MT} is the smallest of all atomic sphere radii in each system. The charge density was Fourier expanded up to $G_{max} = 15$. The following states were considered as valence: RE ($4f$, $5d$, $6s$, $6p$), Rh ($4d$, $5s$, $5p$), X ($5s$, $5p$, $5d$). The specified valence states were treated using the APW+lo scheme while the standard LAPW basis functions were used for all higher angular momentum states in the expansion of the wave function. Local orbitals were added to account for the following semicore states: RE ($4d$, $5s$, $5p$), Rh ($4s$, $4p$), X ($4s$, $4p$, $4d$). The core levels were described using a four-component fully relativistic Dirac solver, while for valence states relativistic effects were included in a scalar relativistic manner [34]. The Brillouin zone sampling was based on 198 **k**-points in the irreducible wedge (2000 points in the full zone). The Kohn-Sham equations were solved within the generalized gradient approximation (GGA) in the form proposed by Perdew, Burke and Ernzerhof [35]. The strong correlation interactions within the Ce $4f$ shell were treated also using the GGA+U approach introduced by Anisimov et al. [36], with an approximate correction for the self-interaction. The exchange constant J for the Ce $4f$ states was assumed $\sim$1eV. The effective U_{eff} is defined as $U_{eff} = U - J$, where U is the Coulomb correlation parameter for the specified shell. The U values between 2 eV and 20 eV have been studied.

Additionally, the full-potential local-orbital minimum basis code (FPLO) [37] was used. The scalar-relativistic calculations were carried out within the local spin density approximation (LSDA) with the parametrization of Perdew Wang [38]. As basis set, RE($4f5s5p/5d6s6p$), Rh($4s4p/4d5s5p$) and Sn($4s4p4d/5s5p$:$5d$) states were employed as semi-core/valence:polarization states. The resulting total electronic densities of states were basically identical for the two band structure codes.

Based on the FPLO results we calculated the theoretical XPS valence band spectra. The partial l-resolved densities of states were multiplied by the corresponding cross sections [39] and convoluted by Lorentzians with a full width at half maximum of 0.4 eV to account for the instrumental resolution, thermal broadening and the effect of the lifetime of the hole states. The results were convoluted by the Fermi-Dirac function for $T = 300$ K.

3 Results and discussion

3.1 Electronic band structure calculations

Figure 2 shows the total and partial atom-resolved DOSs for CeRhIn, CeRhSn as well as for their reference compounds LaRhIn and LaRhSn, calculated within the GGA approximation. Our GGA results for CeRhSn are in a

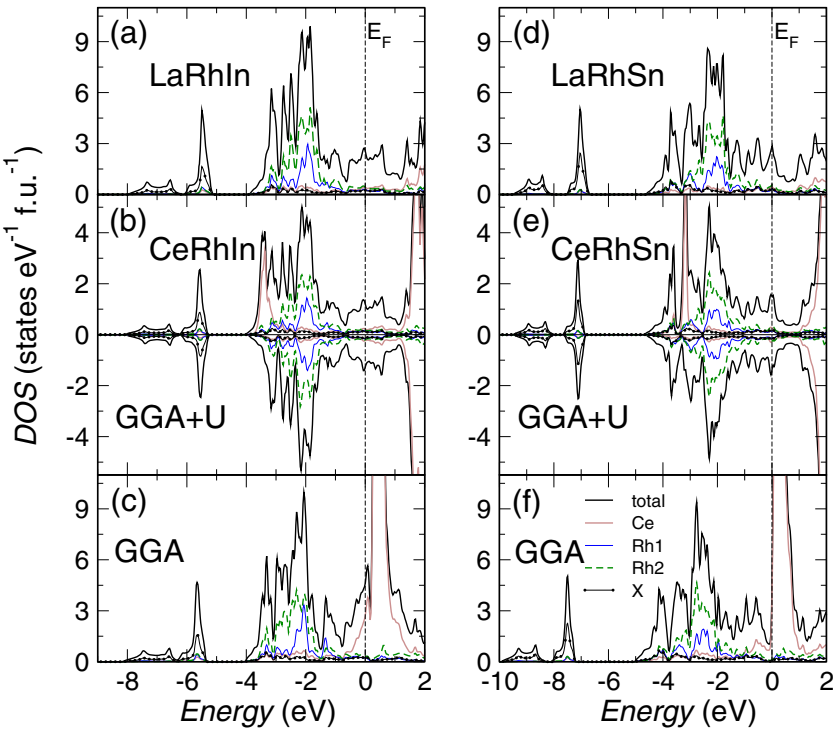

Fig. 2. (Color online) The calculated (LAPW) total and atom resolved densities of states for the compounds LaRhIn (a), CeRhIn (b, c), LaRhSn (d) and CeRhSn (e, f). The common vertical dash lines indicate the position of the Fermi level.

resonable agreement with previous calculations [40–42]. The spin-polarized band structure calculations with initial spin polarization converged back to a nonmagnetic ground state for all investigated compounds. This result is consistent with experimental findings [4,17] and supports the scenario that for CeRhSn the low-temperature magnetism observed for some polycrystalline samples only arises from disorder effects, as suggested previously [16,17].

The valence band for the compounds RERhX consist of two parts separated by the gap of 1–2 eV. The structure at binding energies ranging from 5 to 8 eV or from 6.5 eV to 10 eV for the compounds RERhIn or RERhSn, respectively, originate primarily from the 5s states of the X-elements. The main part of the valence DOS is dominated by the hybridized Rh 4d and X 5p states. For the compounds with Sn this part of conduction band reaches higher binding energies than for the systems with In. The GGA approximation, however, underestimates the Coulomb repulsion for the 4f states, which in this approach form the unrealistic narrow bands close to the Fermi level. Thus, the calculated DOSs (Figs. 2c, 2f) and band structures (Figs. 4c, 4f) result in a too strong hybridization between the 4f and the other conduction band states in the vicinity of the Fermi level for both CeRhIn and CeRhSn.

In order to investigate the influence of the strong correlation interaction within the 4f shell on the electronic structure of the compounds CeRhX, we performed additional band structure calculations using the so-called GGA+U approach. This method simulates the Coulomb repulsion among f electrons in a mean field like (static) approximation. Inclusion of the Hubbard-type interaction term to the XC potential for the Ce 4f states leads to a shift of the occupied Ce 4f bands towards higher binding energies and of the unoccupied 4f states above the Fermi level. Consequently, it strongly suppresses the hybridization between the 4f and valence band states. One should note that this hybridization is crucial for the physical properties of the strongly correlated f-electron systems. For CeRhSn, there is also a significant shift of the other valence band states arising from the changes in the Ce 4f bands induced by application of the GGA+U approach (Fig. 2). Our results are in contrast to previous LDA+U calculations by Matar et al. [41]. There basically no significant shift of states in the DOS was observed, whereas our calculations always result in splits of the order of U_{eff}.

For the U-values larger than ∼3.5 eV the occupied 4f states form a narrow band below the Fermi level. There is still, however, some distinct contribution of the 4f states near the Fermi level due to the hybridization with conduction band states for both CeRhIn and CeRhSn. The traces of such hybridization can be seen in Figures 4b, 4e. It is worthwhile to note that an increase of the U-value leads to the distinct suppression of the admixture of the 4f character in bands close to the Fermi level for the majority spin-channel, while for the minority states this contribution remains significant even for the calculations

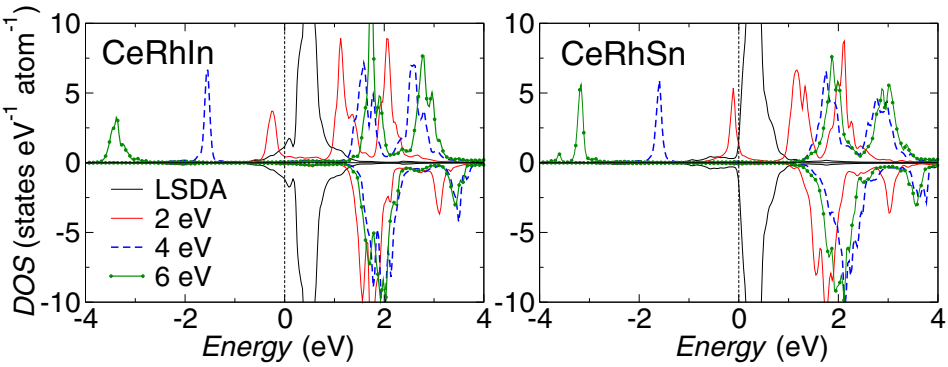

Fig. 3. (Color online) The partial Ce $4f$ DOSs for the compounds CeRhIn and CeRhSn calculated within the GGA approximation or using the GGA+U approach with different values of the U_{eff} parameter equal to 2 eV, 4 eV and 6 eV. Detailed description as in Figure 2.

Table 2. The comparison of the structural data acquired from the LDA and LSDA+U (U_{eff} = 6 eV) calculations for the compounds RERhX (RE = La or Ce; X = In or Sn). The theoratically obtained lattice parameters a, c and internal coordinates x_{RE}, x_X were rounded to 3 significant digits. The table presents also the differences between the experimental and theoretical unit cell volume ΔV.

Compound:	LaRhIn	CeRhIn		LaRhSn	CeRhSn	
	LDA	LDA	LSDA+U	LDA	LDA	LSDA+U
a (Å)	7.488	7.388	7.456	7.402	7.350	7.438
c (Å)	4.102	3.990	4.071	4.181	4.032	4.087
x_{RE}	0.589	0.590	0.591	0.585	0.588	0.589
x_X	0.247	0.252	0.250	0.247	0.254	0.251
V (Å^3)	199.201	188.618	195.965	198.376	188.611	195.825
ΔV (%)	∼4.1	∼6.0	∼2.0	∼3.1	∼4.0	∼0.2

with U_{eff}-values much larger than 6 eV. This indicates the strong hybridization of the $4f$ and conduction band states for both CeRhIn and CeRhSn. Furthermore, for a reasonable range of U_{eff} values (3.5–7 eV [43]) the unoccupied Ce $4f$ states remain almost unchanged (Fig. 3). To inspect the unoccupied states in both CeRhSn and CeRhIn, bremsstrahlung isochromat spectroscopy (BIS) studies are strongly suggested.

We are aware of the fact that none of our calculations (GGA or GGA+U) gives a fully satisfactory description of the electronic structure for the compounds CeRhIn and CeRhSn in a region close to the Fermi level, where dynamic many body effects play an essential role for the physical properties. Nevertheless, the band structures derived from the density functional theory calculations unequivocally revealed a strong hybridization between the Ce $4f$ and conduction band states for both CeRhSn and CeRhIn. The analysis of partial weights of the band states (not shown) clearly indicates that in CeRhSn the Ce $4f$ states hybridize mainly with the $4d$ states of Rh2, while for CeRhIn we find is a significant hybridization of the $4f$ states with the states of both Rh1 and Rh2. Furthermore, the calculated DOSs (Fig. 2) show that replacement of In by Sn results in a slight shift of the Rh $4d$ bands towards higher binding energies due to the hybridization with the Sn $5p$ states. This points to the stronger covalency of bonds between atoms of Rh and Sn in both LaRhSn and CeRhSn.

Finally, we performed a computational crystal structure optimization for all the compounds RERhX (RE = La, Ce; X = In, Sn). The full structures relaxation was carried out using the FPLO code due to the high numerical efficiency of this computational scheme. The experimental crystallographic data were taken as a starting point (see Tab. 1). The unit cell volume, the c/a ratio and the internal coordinates for each compound were optimized successively in at least four full cycles. In case of the compounds CeRhIn and CeRhSn we applied the LDA approximation as well as the LSDA+U approach for the Ce $4f$ states. The resulting lattice parameters and atomic positions are listed in Table 2. The FPLO derived internal coordinates we cross-checked using the WIEN2k computer code, in which the atomic forces were calculated according to the method proposed by Yu et al. [44]. For the optimized atomic positions we obtained total forces on each atom smaller than 5 mRy/a.u. All the theoretical atomic coordinates are in good agreement with the experimental results (Tab. 1). It should be stressed that there is a significant difference in equilibrium unit cell volume for both CeRhIn and CeRhSn between the results obtained within the LDA and LSDA+U approximation (∼4%). This indicate that the Ce $4f$ electrons contribute essentially to the chemical bonding in these systems. The LDA lattice

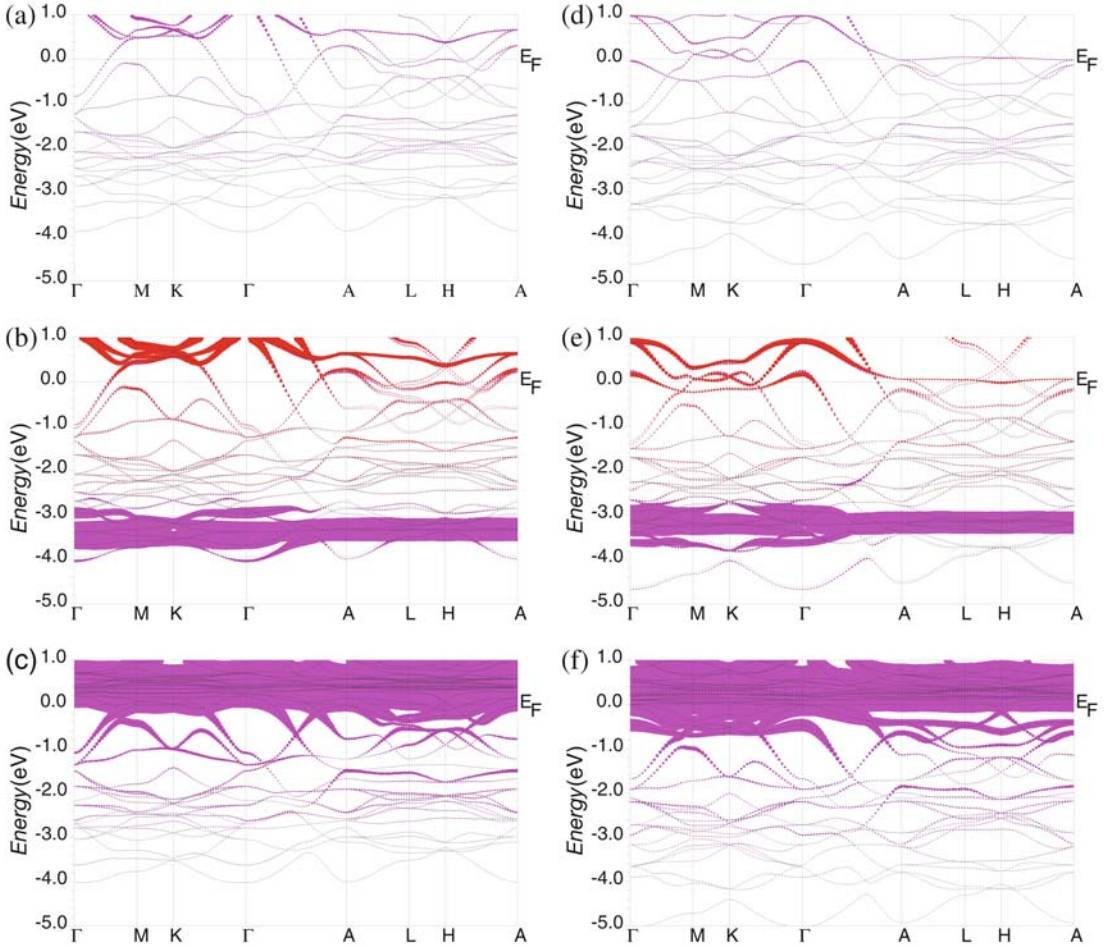

Fig. 4. (Color online) Electronic band structure close to the Fermi level for LaRhIn (a), CeRhIn (b, c), LaRhSn (d) and CeRhSn (e, f) calculated within the GGA approximation (a, c, d, f) or using the GGA+U approach with U_{eff} = 6 eV (b, e). The size of the points denotes the weights of the RE 4f contributions. The high symmetry points are labelled according to the standard notation.

parameters for both CeRhIn and CeRhSn show stronger deviation from the experimental data than that for the reference compounds LaRhIn and LaRhSn due to the overestimation of the 4f contribution to the bonds. In contrast, the LSDA+U method results in a significantly larger unit cell volumes due to the overestimated suppression of the hybridization between the Ce 4f and conduction band states. Hence, the equilibrium lattice parameters obtained using this approach do not show the contraction typical for the LDA approximation. Such a contraction is clearly visible for the compounds LaRhIn and LaRhSn.

To gain deeper inside into the chemical bonding we analyse the charge density distribution in the compounds RERhX (RE = La, Ce; X = In, Sn).

3.2 Charge density analysis

The reordering of electronic charge density accompanying the bonding formation in solids can be well visualized using the difference charge density plots. Such maps are calculated by subtracting the superposition of free atom densities from the total crystalline valence charge density. The results for the compounds RERhX (RE = La, Ce; X = In, Sn) are presented in Figure 5.

For CeRhIn (Fig. 5a) the difference charge density maps show that electrons are accumulated mainly between the pairs of the nearest neighbouring (NN) atoms: Ce–Rh1 (labeled A in Fig. 5) and Ce–Rh2 (labeled C in Fig. 5). This points to the covalent-like bonds between Ce and Rh atoms in the *ab* planes and along the hexagonal axis.

Replacement of the In atoms by Sn, which has one valence electron more, results in an essential redistribution of the valence charge density. It leads to: (i) the creation of the charge accumulations between the pairs of the NN Rh2 and Sn atoms (labeled B in Fig. 5); (ii) the substantial increase in electron density around the Rh1 atoms, towards the region between the surrounding Sn atoms (labeled E in Fig. 5). The first effect can be attributed to the formation of the strong covalent-like bonds in the *ab* plane, between the NN Rh2 and Sn atoms. These bonds are presumably responsible for the observed shrinking of the lattice parameter a for both LaRhSn and CeRhSn

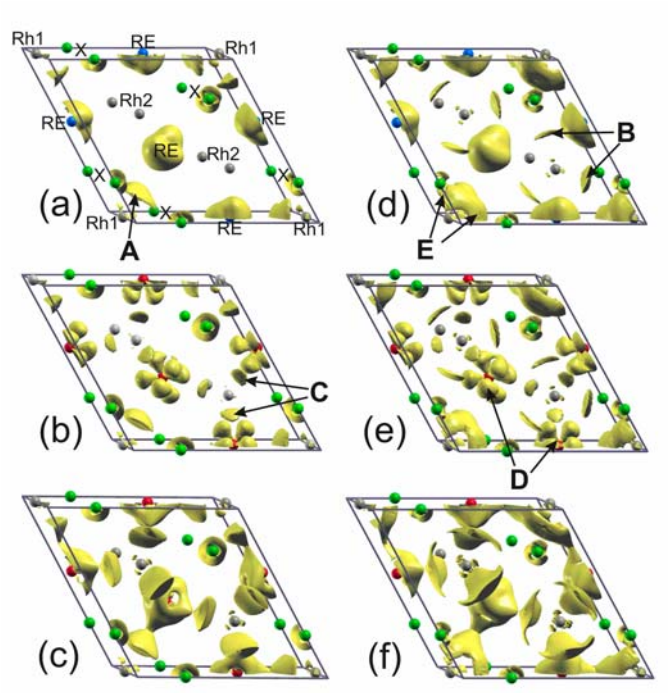

Fig. 5. (Color online) The surface of constant difference charge density equal to 0.0047 (electron/a.u.^{3}) for LaRhIn (a), CeRhIn (b, c), LaRhSn (d) and CeRhSn (e, f) calculated within the GGA approximation (a, c, d, f) or using the GGA+U (U_{eff} = 6 eV) approach. Because of symmetry, only half of the unit cell is considered. Labels (A, B, C, D, E) see text.

with respect to the corresponding indides (Tab. 1). The second observation indicates the creation of some multi-center-type bonds between one Rh1 and two NN Sn atoms situated above and below this Rh1. Thus, the difference charge density maps point to the more covalent character of the investigated stannides than the indides, which corroborates the analysis of the DOSs presented in Section 3.1.

To get insight into the role of Ce 4f electrons in formation of the bonds in both CeRhIn and CeRhSn we have calculated difference charge density plots based on the band structure results obtained within the GGA approximation as well as using the GGA+U approach for the Ce 4f states with different values of the U-parameter. The exemplary plots calculated using the GGA and GGA+U (U_{eff} = 6 eV) methods are shown in Figure 5. The comparative analysis of the density maps revealed that there is a distinct 4f contribution to the covalent-like bonds between the Ce and Rh2 atoms, similar in CeRhIn and CeRhSn, arising from the hybridization between the 4f and conduction band states in the vicinity of the Fermi level. One should note that the electron density plots for the reference compounds LaRhIn and LaRhSn do not show strengthened charge density between the La and Rh2 atoms, which corroborates the essential 4f contribution to the creation of these Ce–Rh2 bonds. Furthermore, for the indides the charge accumulations between the RE and Rh1 atoms are more pronounced in CeRhIn than in LaRhIn and for CeRhIn the number of assembled electrons in these regions decreases with increase of the U value in the GGA+U approach. This points to the signficant 4f contribution in these bonds for the compound CeRhIn. In contrast, in the stannides there is no distinct difference in charge density distribution in regions between the RE and Rh1 atoms for CeRhSn and LaRhSn. Moreover, for a reasonable range of the U_{eff}-values (3.5–6 eV) we did not find an influence of the applied U-value on the electron density in these regions in CeRhSn. These findings indicate that for CeRhSn the Ce 4f states participate substantially in the formation of bonds with Rh2 atoms, as suggested based on the analysis of the partial weights of the band states (see discussion in Sect. 3.1).

It should be stressed that for both CeRhIn and CeRhSn the GGA approximation results in the substantial accumulations in the binding region related to the Ce and leads to the delocalization of the 4f electron density. In contrast, the GGA+U approach yields the distinct features marked as D in Figure 5, which originate primarily from the 4f electron density localized on the Ce atoms. Hence, their form reflects the shape of the occupied 4f orbitals.

3.3 XPS results

Information about the character of the Ce 4f states in Ce-based intermetallics at ambient temeprature can be efficiently derived from the Ce core-level XPS spectra owing to the strong Coulomb interaction between the photoemission core-hole and the electrons near the Fermi level. This coupling results in a complex structure of the Ce

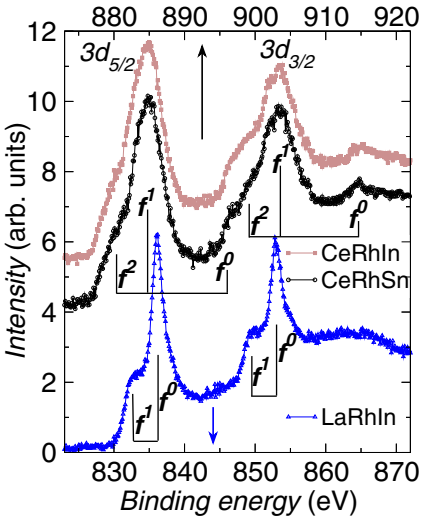

Fig. 6. (Color online) The RE 3*d* XPS spectra for CeRhSn, CeRhIn and its reference compound LaRhIn. The shoulder in the spectrum of LaRhIn at ∼865 eV originates from the La MNN Auger line.

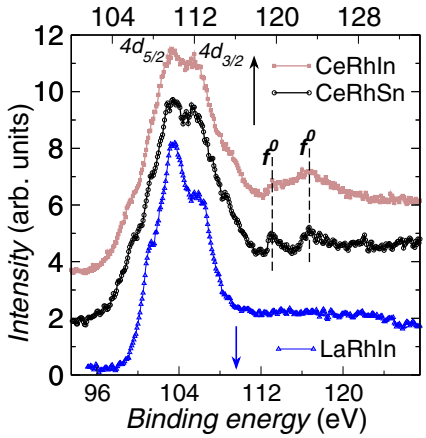

Fig. 7. (Color online) The RE 4*d* XPS spectra for CeRhSn, CeRhIn and LaRhIn. In the spectra of RERhIn there are also wide peaks originating from the In 4*s* states at ∼123 eV.

core-level XPS spectra. A detailed examination we restrict to the most intensive peaks related to the photoemission from Ce 3*d* and 4*d* states since the lifetime broadening of the other levels masks fine structures originating from screening effects. For a comparison, we present also the XPS spetra of the reference compound LaRhIn.

Figure 6 shows the RE 3*d* XPS spectra of CeRhSn, CeRhIn and LaRhIn. The spin-orbit (SO) splitting of the final 3*d* states results in two sets of photoemission lines in each spectrum with an intensity ratio

$$I(3d_{5/2}) \;/\; I(3d_{3/2}) \;=\; 3/2. \qquad (1)$$

The estimated values of the SO splitting ($\delta_{\mathrm{Ce}} \approx 18.6$ eV, $\delta_{\mathrm{La}} \approx 17.3$ eV) are in agreement with those obtained from our band structure calculations ($\delta_{\mathrm{Ce}} \approx 18.8$ eV, $\delta_{\mathrm{La}} \approx 17.2$ eV). Each set of photoemission lines consists of several contributions corresponding to the different occupation of the Ce 4*f* shell in a final state. The main peaks, marked as f^0 and f^1 for La and Ce, respectively, originate from a screening of the core-hole by conduction electrons. These peaks are much wider for CeRhSn and CeRhIn than for LaRhIn due to the multiplet effects, as well as a special broadening mechanism related to the so-called virtual-bound-state effects [45]. The satellites located on the low-energy side of the main photoemission lines appear when the core-hole becomes screened by an extra 4*f* electron in an exciton-like level centered on the core-ionized atom owing to a $4f^n \rightarrow 4f^{n+1}$ transition during the photoemission process. The probability of transferring an electron to this screening level strongly depends on its coupling to the other occupied states. Therefore the contributions in the measured RE 3*d* XPS spectra labelled as f^1 and f^2 for La and Ce, respectively, can be considered as an indicator of the hybridization strength between the 4*f* and the conduction band states. In the Ce 3*d* XPS spectra of CeRhSn and CeRhIn there are also distinct peaks in a distance of about 11 eV from the main photoemission lines. These contributions originate from the f^0 final states and point to an intermediate valence behaviour of Ce in both compounds. In the analysed spectra one can expect also additional contributions related to the photoemission from the 3*s* states of In and Sn, located at binding energies of 828 eV and 885 eV, respectively. These peaks, however, should be very broad and weak due to the small photoemission cross section for these states [39] and thus they could not be clearly resolved.

The quantitative analysis of the RE 3*d* XPS spectra we performed based on the Gunnarsson and Schönhammer (GS) model calculations [46,47]. The separation of the overlapping peaks in the XPS spectra we made on a basis of the Doniach-Šunjić theory [48], after subtraction of the background calculated using the Tougaard algorithm [49]. According to the GS model, one can estimate the occupation number of the Ce 4*f* shell in the initial state n_f^{XPS} using Figure 4 of the reference [46] and the ratio

$$r = I(f^0)/(I(f^0) + I(f^1) + I(f^2)), \qquad (2)$$

where $I(f^n)$ is the intensity of the f^n peak. For CeRhSn and CeRhIn we obtained $n_f^{XPS} \approx 0.93$. This value indicates that the average valence of Ce ions $v^{XPS} \approx 3.07$ for both investigated compounds. In order to get insight into the strength of the hybridization between the RE 4*f* and the conduction band states we estimated the values of the Δ parameter. This parameter is defined as $\pi V^2 \rho_{max}$, where ρ_{max} is the maximum value of the DOS and V is the hybridization matrix element in the Anderson impurity Hamiltonian. We calculated the ratio

$$R = I(f^2)/(I(f^1) + I(f^2)) \qquad (3)$$

and used Figures 5 and 6 of reference [46], assuming the conduction band DOS to be a simple semielliptic with lower edge $B^- = -4$ eV and upper edge $B^+ = 1.57$ eV with respect to the Fermi level. The same procedure applied for the RE 3*d* XPS spectra of LaRhIn, CeRhIn and CeRhSn yielded $\Delta \approx 120$ meV for La and $\Delta \approx 100$ meV

for Ce in both CeRhIn and CeRhSn. One should note that the large values of hybridization energy $\Delta \sim 100$ meV are typical for Ce-based intermediate valence compounds [46,50]. For CeRhSn the estimated values of the parameters Δ and n_f^{XPS} are consistent with those previously reported [16].

A valence fluctuation state of Ce ions in CeRhSn and CeRhIn has been also confirmed by the Ce $4d$ XPS spectra (Fig. 7). In these spectra one can clearly see the two peaks in a distance of 11 eV from the main photoemission maxima. These contributions can be assigned to the $4d^9 4f^0$ final states and give evidence for an intermediate-valence state of Ce. In case of CeRhIn these satellites overlap with the additional very wide feature at about 124 eV related to the photoemission from the In $4d$ states. Analogous slight contribution can be observed in the spectrum of LaRhIn. The main structure in the RE $4d$ XPS spectra at binding energies ranging from 104 eV to 118 eV consists of two sets of photoemission lines originating from $4d^9 4f^n$ and $4d^9 4f^{n+1}$ ($n = 0$ for La, $n = 1$ for Ce) final states, whose separation corresponds to the core-hole $4d$ spin-orbit interaction $\delta_{\mathrm{Ce}} \approx 3.2$ eV, $\delta_{\mathrm{La}} \approx 3.0$ eV. For Ce the detailed analysis of this region is not possible due to the strong exchange interaction between $4d$ holes and the unfilled $4f$ levels, which gives rise to complicated multiplet structures [51]. Nevertheless, one can clearly see that the shape of the main photoemission lines in the Ce $4d$ XPS spectra of CeRhSn and CeRhIn is very similar, which is in line with their indistinguishable values of the Δ and n_f^{XPS} parameters derived from the Ce $3d$ XPS spetra. Furthermore, there are no noticeable differences in shape and energy position of the main photoemission lines as well as the satellites in the Ce $3d$ XPS spectra of CeRhSn and CeRhIn. This findings point to the very similar character of the Ce $4f$ states at ambient temperature in both compounds.

Further insight into the electronic structure at ambient temperature can be gained from the XPS valence band spectra (Fig. 8). The recorded data we interpret with the help of band structure calculations. Based on the partial DOSs and photoemission cross-sections given by Yeh and Lindau [39] we have estimated the photoemission spectra, according to the description in Section 2.2. We utilized the DOSs obtained by the FPLO code, since the LAPW computational scheme demands the presence of electrons in the interstitial region, which cannot be taken straightforwardly into account in a simulation of the theoretical XPS spectra. The results are presented in Figure 8.

The main peak in valence band spectra, located at about 2–2.5 eV, originates mainly from the Rh $4d$ states hybridized with the $5p$ states of X-element. The second peak centered at about 5.6 eV or 7.5 eV for the compounds RERhIn and RERhSn, respectively, is related to photoemission from the $5s$ states of In or Sn. In order to expose the "pure" Ce $4f$ contributions to the XPS valence band spectra we plotted also the partial Ce $4f$ DOSs as well as the sum of all partial l-resolved DOSs, multiplied by the corresponding cross-sections. The exemplary results obtained for CeRhIn based on the DOSs

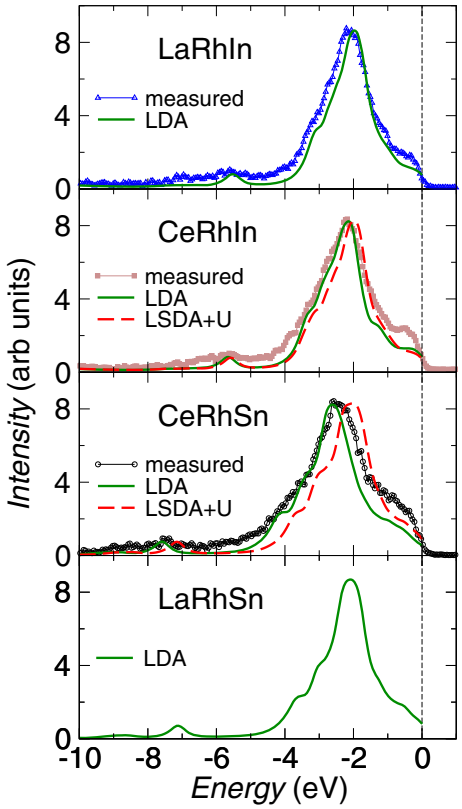

Fig. 8. (Color online) Comparison of the experimental XPS valence band spectra, corrected by the background estimated according to the Tougaard algorithm [49] (line with points), with the theoretical ones estimated based on the DOSs calculated using the FPLO code within the LDA approximation (dash line) and using the LSDA+U approach with $U_{eff} \approx 6$ eV (solid line).

resulting from the LSDA+U calculations are presented in Figure 9. It is clearly visible that photoemission from the $4f$ states should give only a small contribution to the measured spectra, as compared to the other valence band states. Therefore the XPS valence band spectra cannot give unequivocal information about the localization of the $4f$ states in valence band for the compounds CeRhX.

The theoretical simulations reproduce well the overall shape of the XPS valence band spectra for all investigated compounds. For LaRhIn, the slight distinction between the calculated and measured intensity in the vicinity of the Fermi level presumably originates from the inadequacy of the atomic-like photoemission cross sections for the valence band states of intermetallic compounds (see discussion in Refs. [52,53]). For CeRhIn and CeRhSn, however, the discrepancy is considerably larger which suggests that there is an additional contribution to the measured DOS in the vicinity of the Fermi level. We suppose that this contribution arises primarily from a peak of the electronic quasi-particle DOS near the Fermi level due to an Abrikosov-Suhl resonance. It is worthwhile to stress that the LSDA+U approach is a static mean-field approximation. Consequently, this method can not reproduce dynamic many-body effects. For CeRhIn the presence of the

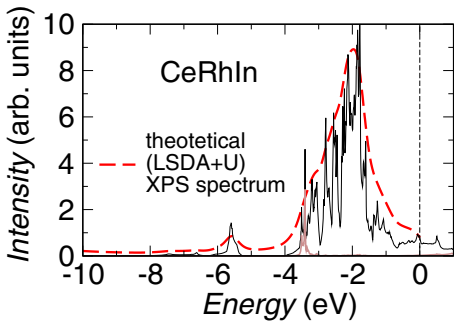

Fig. 9. (Color online) The theoretical XPS valence band spectrum for the compound CeRhIn obtained based on the DOSs calculated using the FPLO code within the LSDA+U ($U_{eff} \approx 6$ eV) approximation. The thin solid black line represents the sum of the partial l-resolved DOSs multiplied by the corresponding cross-sections. The thick solid grey (brown) line shows the partial Ce $4f$ contribution.

Kondo-peak in the valence band at ambient temperature is in line with the high Kondo temperature of at least about 300 K [4]. On the other hand, in case of CeRhSn, different experimental results evaluated with different models pointed to a lower Kondo temperature (about 140 K [16], 240 K [17], 40 K [4]). Hence, at ambient temperature the Kondo resonance should decay.

We observe a slight shift of the peak positions between the experimental and the calculated XPS valence band spectra of LaRhIn (Fig. 8). It is well known that the real (incomplete) screening of a photoemission hole can not be described in ground state calculations. This effect leads to a slightly smaller kinetic energy of the emitted photoelectrons and consequently to a tiny shift of the measured XPS peaks toward higher binding energies. Since the overall shape of the valence band is very similar for all investigated compounds, one can expect the analogous effects in the XPS spectra of CeRhIn and CeRhSn. Furthermore, the detailed analysis of thermal expansion for the compound CeRhSn suggests that there is a change in bonding versus temperature in this system at the temperature of 120 K, presumably related to the Ce valence instability. This prevents us from performing any more comprehensive comparative analysis of the theoretical and experimental XPS valence band spectra for the compounds RERhX. One should note, that for CeRhSn the position of the main peaks in theoretical XPS valence band depends considerably on the treatment of the Ce $4f$ states in band structure calculations due to their hybridization with the other valence band states. Thus, valence band photoemission at low temperatures should give additional information about the hybridization of the $4f$ and the conduction band states for this compound.

3.4 Discussion and summary

At ambient temperature the electronic structure of Ce related states is very similar in CeRhIn and CeRhSn. The Ce core-level XPS spectra revealed intermediate valence state of the Ce ions and a strong hybridization of the $4f$ and the conduction band states $\Delta \approx 100$ meV for both investigated compounds. In contrast, the high-resolution $3d$–$4f$ resonance photoemission studies performed at a temperature of 15 K indicated that the hybridization between the $4f$ and the other valence band states is distinctly weaker for CeRhSn than for CeRhIn [20]. This provides an explanation for the discrepancy in the low-temperature thermodynamic and transport properties of these compounds [4,16].

The detailed analysis of the ground state electronic structures based on the ab initio calculations indicates that there is a substantial hybridization of the $4f$ and conduction band states for both CeRhIn and CeRhSn. However, for CeRhSn the Ce $4f$ states hybridize mainly with the states of Rh2, while in case of CeRhIn there is a significant hybridization with the states of both Rh1 and Rh2. This outcome is supported by the difference charge density plots, which revealed that for CeRhSn the Ce $4f$ states participate mainly in the formation of bonds with Rh2 atoms. In turn, in case of CeRhIn we found a pronounced contribution of the $4f$ states to the formation of bonds with both Rh1 and Rh2.

The presented results indicate that there should be some change in the character of the Ce $4f$ states in CeRhSn at temperatures below 300 K. Indeed, for this compound the thermal expansion of the crystal lattice shows an anomaly, which is clearly visible in the $c/a(T)$ plot at about 120 K [16]. The careful analysis of the temperature dependent changes in interatomic distances revealed that the anomaly is related primarily with the planar Ce–Rh1 bonds [16]. In contrast, for CeRhIn we found the linear dependence of the lattice parameters versus temperature in a wide temperature range (Fig. 1). It should be noted that for the temperature dependence of the c/a ratio the total error bars cover the deviation of the experimental points from the straight line.

Finally, the difference charge density plots point to the formation of pronounced covalent-like bondings betweeen Sn–Rh1 and Sn–Rh2 atoms in both LaRhSn and CeRhSn. The stronger covalency of the investigated stannides is also visible in the calculated DOSs and is presumably responsible for the markedly smaller thermal lattice-expansion for CeRhSn than for CeRhIn. Furthermore, replacement of In by Sn atoms leads to a distinct shrinking of the lattice parameter a accompanied by the increase in the c parameter for both LaRhX and CeRhX, which can be assigned to the characteristic covalent bonding situation. It is worthwhile to stress, that all the changes in the experimental lattice parameters for the whole family of compounds RERhX (RE = La, Ce; X = In, Sn) depending on RE and X are at least qualitatively reflected also in the equilibrium lattice parameters derived from the theoretical calculations, which supports the reliability of our band structure results.

To summarize, we have investigated the electronic structure of the compounds RERhX (RE = La, Ce; X = Sn, In) based on the XPS measurements and the DFT band structure calculations. The XPS spectra revealed an intermediate valency of the Ce ions in both CeRhSn and

CeRhIn and the substantial hybridization of the $4f$ and the conduction electrons. Both compounds behave similar at ambient temperature, although CeRhSn exhibits more covalent character of the chemical bonding. At low temperatures the differences between the two compounds are more pronounced. Whereas CeRhIn shows typical temperature dependence of the thermodynamical and structural properties, CeRhSn displays distinct anomalies. For a further understanding of these differences, new experiments like BIS and temperature dependent photoemission would be desirable.

The authors thank Marek Kulpa for help with XPS measurements. The authors also thank for financial support from Projects Nos. 1 P03B 052 28, N202 010 32/0487 of Ministry of Science and Higher Education and for the DFG, Emmy Noether-program.

References

1. A. Szytuła, B. Penc, Ł. Gondek, Acta Phys. Pol. A **111**, 475 (2007)
2. L. Menon, A. Agarwal, S.K. Malik, Physica B **230**, 201 (1997); N.C. Tuan, V. Sechovský, M. Diviš, P. Svoboda, H. Nakotte, F.R. de Boer, N.H. Kim-Ngan, J. Appl. Phys. **73**, 5677 (1993)
3. R.K. Singhal, N.L. Saini, K.B. Garg, J. Kanski, L. Ilver, P.O. Nilsson, J. Phys.: Condens. Matter **5**, 4013 (1993)
4. H. Higaki, I. Ishii, D. Hirata, M.-S. Kim, T. Takabatake, T. Suzuki, J. Phys. Soc. Jpn **75**, 024709 (2006)
5. D.T. Adroja, S.K. Malik, B.D. Padalia, R. Vijayaraghavan, Phys. Rev. B **39**, 4831 (1989)
6. A.M. Strydom, S. Paschen, F. Steglich, Physica B **378–380**, 793 (2006)
7. Y. Bando, T. Suemitsu, K. Takagi, H. Tokushima, Y. Echizen, K. Katoh, K. Umeo, Y. Maeda, T. Takabatake, J. Alloys Comp. **313**, 1 (2000); P. Salamakha, O. Sologub, J.L. Yakinthgos, Ch.D. Routsi, J. Alloys Comp. **181**, 111 (1992)
8. K. Satoh, T. Fujita, Y. Maeno, Y. Uwatoko, H. Fujii, J. Phys. Soc. Jpn **59**, 692 (1990)
9. T. Fujita, K. Satoh, Y. Maeno, Y. Uwatoko, H. Fujii, J. Magn. Magn. Mat. **76, 77**, 133 (1988)
10. E. Brück, M. Van Sprang, J.C.P. Klaesse, F.R. De Boer, J. Appl. Phys. **63**, 3417 (1988); B. Chevalier, A. Wattiaux, J.-L. Bobet, J. Phys.: Condens. Matter **18**, 1743 (2006)
11. A. Dönni, G. Ehlers, H. Maletta, P. Fischer, H. Kitazawa, M. Zolliker, J. Phys.: Condens. Matter **8**, 11213 (1996); L. Keller, A. Dönni, H. Kitazawa, B. van Brandt, Appl. Phys. A **74**, S686 (2002)
12. A. Oyamada, S. Maegawa, M. Nishiyama, H. Kitazawa, Y. Isikawa, Phys. Rev. B **77**, 064432 (2008)
13. R. Movshovich, J.M. Lawrence, M.F. Hundley, J. Neumeier, J.D. Thompson, A. Lacerda, Z. Fisk, Phys. Rev. B **53**, 5465 (1996)
14. B. Chevalier, J.-L. Bobet, Intermetallics **9**, 835 (2001); P. Javorsky, A. Chernyavsky, V. Sechovsky, Physica B **281, 282**, 71 (2000)
15. Ł. Gondek, A. Szytuła, B. Penc, J. Hernandez-Velasco, A. Zygmunt, J. Magn. Magn. Mat. **262**, L177 (2003)
16. A. Ślebarski, M.B. Maple, E.J. Freeman, C. Sirvent, M. Radłowska, A. Jezierski, E. Granado, Q. Huang, J.W. Lynn, Philos. Mag. B **82**, 943 (2002)
17. M.S. Kim, Y. Echizen, K. Umeo, S. Kobayashi, M. Sera, P.S. Salamakha, O.L. Sologub, T. Takabatake, X. Chen, T. Tayama, T. Sakakibara, M.H. Jung, M.B. Maple, Phys. Rev. B **68**, 054416 (2003)
18. P.-C. Ho, V.S. Zapf, A. Ślebarski, M.B. Maple, Philos. Mag. **84**, 2119 (2004)
19. H. Tou, M.S. Kim, T. Takabatake, M. Sera, Phys. Rev. B **70**, 100407(R) (2004)
20. K. Shimada, H. Namatame, M. Taniguchi, M. Higashiguchi, S.-I. Fujimori, Y. Saitoh, A. Fujimori, M.S. Kim, D. Hirata, T. Takabatake, Physica B **378–380**, 791 (2006)
21. K. Łątka, R. Kmieć, A.W. Pacyna, R. Pöttgen, J. Magn. Magn. Mat. **320**, L18 (2008)
22. R.B. Griffiths, Phys. Rev. Lett. **23**, 17 (1969)
23. A.H. Castro Neto, G. Castilla, B.A. Jones, Phys. Rev. Lett. **81**, 3531 (1998)
24. R. Ferro, R. Marazza, G. Rambaldi, Z. Anorgan. Allgem. Chemie **410**, 219 (1974)
25. P. Raj, A. Sathyamoorthy, K. Shashikala, C.R. Venkateswara Rao, D. Kundaliya, S.K. Malik, J. Alloys Comp. **345**, L1 (2003); S.K. Malik, D. Kundaliya, A. Sathyamoorthy, K. Shashikala, P. Raj, V.V. Krishnamurthy, J. Appl. Phys. **93**, 7843 (2003)
26. D. Rossi, D. Mazzone, R. Marazza, R. Ferro, Z. Anorgan. Allgem. Chemie **507**, 235 (1983)
27. F. Canepa, S. Cirafici, J. Alloys Comp. **232**, 71 (1996)
28. B. Chevalier, C.P. Sebastian, R. Pöttgen, Solid State Sciences **8**, 1000 (2006)
29. W. Krauss, G. Nolze, J. Appl. Cryst. **29**, 301 (1996)
30. J. Laugier, B. Bochu, *Checkcell: Graphical Powder Indexing, Cell and Space Group Assignment Software*, `http://www.inpg.fr/ LMGP`
31. Y. Baer, G. Bush, P. Cohn, Rev. Sci. Instrum. **46**, 466 (1975)
32. D. Singh, *Plane waves, pseudopotentials and the LAPW method* (Kluwer Academic, 1994)
33. P. Blaha, K. Schwarz, G. Madsen, D. Kvasnicka, J. Luitz, *Program for calculating crystal properties* WIEN2k, Vienna University of Technology (2001), ISBN 3-9501031-1-2
34. D.D. Koelling, B N Harmon, J. Phys. C: Sol. St. Phys. **10**, 3107 (1977)
35. J.P. Perdew, K. Burke, M. Ernzerhof, Phys. Rev. Lett. **77**, 3865 (1996)
36. V.I. Anisimov, I.V. Solovyev, M.A. Korotin, M.R. Czyżyk, G.A. Sawatzky, Phys. Rev. B **48**, 16929 (1993); V.I. Anisimov, J. Zaanen, O.K. Andersen, Phys. Rev. B **44**, 943 (1991); V.I. Anisimov, F. Aryasetiawan, A.I. Lichtenstein, J. Phys.: Condens. Matter **9**, 767 (1997)
37. K. Koepernik, H. Eschrig, Phys. Rev. B **59**, 1743 (1999)
38. J.P. Perdew, Y. Wang, Phys. Rev. B **45**, 13244 (1992)
39. J.J. Yeh, J. Lindau, At. Data Nucl. Data Tables **32**, 1 (1985)
40. A. Ślebarski, A. Jezierski, Phys. Stat. Sol. (b) **236**, 340 (2003)
41. S.F. Matar, J.F. Riecken, B. Chevalier, R. Pöttgen, A.F. Al Alam, V. Eyert, Phys. Rev. B **76**, 174434 (2007)
42. T. Schmidt, D. Johrendt, C.P. Sebastian, R. Pöttgen, K. Łątka, R. Kmieć, Z. Naturforsch. **60b**, 1036 (2005)

43. Y. Baer, H.R. Ott, J.C. Fuggle, L.E. De Long, Phys. Rev. B **24**, 5384 (1981); J.K. Lang, Y. Baer, P.A. Cox, J. Phys. F **11**, 121 (1981); J.F. Herbst, R.E. Watson, J.W. Wilkins, Phys. Rev. B **17**, 3089 (1978); J.F. Herbst, J.W. Wilkins, Phys. Rev. Lett. **43**, 1760 (1979); V.I. Anisimov, O. Gunnarsson, Phys. Rev. B **43**, 7570 (1991) and references there in
44. R. Yu, D. Singh, H. Krakauer, Phys. Rev. B **43**, 6411 (1991)
45. J.C. Fuggle, O. Gunnarsson, G.A. Sawatzky, K. Schönhammer, Phys. Rev. B **37** 1103 (1988)
46. J.C. Fuggle, F.U. Hillebrecht, Z. Zolnierek, R. Lässer, Ch. Freiburg, O. Gunnarsson, K. Schönhammer, Phys. Rev. B **27**, 7330 (1973); A.J. Signorelli, R.G. Hayes, Phys. Rev. B **8**, 81 (1973)
47. O. Gunnarsson, K. Schönhammer, Phys. Rev. B **28**, 4315 (1983)
48. S. Doniach, M. Šunjić, J. Phys. C **3**, 286 (1970)
49. S. Tougaard, P. Sigmund, Phys. Rev. B **25**, 4452 (1982)
50. A. Ślebarski, A. Jezierski, A. Zygmunt, S. Mähl, M. Neumann, Phys. Rev. B **58**, 13498 (1998)
51. Y. Baer, R. Hauger, Ch. Zürcher, M. Campagna, G.K. Wertheim, Phys. Rev. B **18**, 4433 (1978)
52. M. Gamża, A. Ślebarski, J. Deniszczyk, J. Phys.: Condens. Matt. **20**, 025201 (2008)
53. M. Gamża, W. Schnelle, A. Ślebarski, U. Burkhardt, R. Gumeniuk, H. Rosner, J. Phys.: Condens. Matter, to be published